Optical Scattering from Vitreous Floaters

Stuart W. Harmer,[1]* Andrew J. Luff,[2] and Giampaolo Gini[3]

[1]*Department of Engineering, Computing and Design, University of Chichester, Chichester, UK*
[2]*Sapphire Eyecare, Southampton, UK*
[3]*Western Sussex NHS University Trust, Chichester, UK*

Vitreous "floaters" are a common entoptic phenomenon that can result in significant reduction in quality of life in a proportion of sufferers. The authors use a computational mathematical model based on Fourier optics and reflection and transmission coefficients calculated for a planar type II collagen opacity suspended in aqueous to show that floaters are perceived by the patient through interference effects that result in significant variations in intensity on the retina when viewing a constant brightness surface. The model also predicts that backscattered intensity from floaters is ten thousand to one million times lower than the variations in intensity produced on the retina, which demonstrates that the visible effects of floaters for the patient can be highly significant, whereas clinical observation of the vitreous may be entirely unremarkable. Importantly, the results also demonstrate that floaters do not need to be opaque to cause symptoms, with only small differences in refractive index between the floater material and the surrounding vitreous needed to produce significant optical effects. The model predicts that pupil size is an important factor in determining the severity of symptoms from floaters, with constricted pupils giving much greater effect than dilated pupils. Finally, the authors' model predicts that floaters degrade contrast sensitivity function, with greatest degradation occurring in the 5–40 cycles per degree spatial frequency range and that the effects of shadowing caused by floaters are very strongly correlated to the predicted degradation of contrast sensitivity function.

Keywords: **floaters; vision; scattering; symptomatic vitreous opacity; contrast sensitivity function**

INTRODUCTION

Vitreous floaters are a common entoptic phenomenon that can have a considerable detrimental effect on the quality of life in a small but significant proportion of those that are symptomatic [Sebag, 2011; Wagle et al., 2011; Zou et al., 2013; Luff and O'Donnell, 2018]. The reason for the wide spectrum of tolerance to floater symptoms is unknown, but psychological as well as physical parameters are suspected to play a role [Cipolletta et al., 2012; Wu et al., 2020]. When vitreous floaters produce symptoms, they are often referred to as symptomatic vitreous opacity (SVO) [Ivanova et al., 2016]. In dealing with the symptomatic patient, the ophthalmic community is confronted with the difficulty in reconciling often-unremarkable clinical observations with the occasionally profound symptoms of the patient presenting with SVO [Luff and O'Donnell, 2018]. The difficulty is due to multiple factors, which include: a traditional view that chronic vitreous opacity is trivial and of no medical consequence; the scientifically unsubstantiated belief that vitreous opacity will spontaneously migrate out of the sufferer's visual axis or that the patient will become accustomed to or tolerant of the visual disturbances due to their opacity and the historical lack of safe and effective treatments for SVO, although this is

Conflicts of interest: None.

*__Correspondence__ to: Stuart W. Harmer, Department of Engineering, Computing and Design, the University of Chichester, Chichester PO21 3HR, UK.
Email: s.harmer@chi.ac.uk

Received for review 2 June 2021; Revised 7 December 2021; Accepted 18 December 2021

DOI:10.1002/bem.22386
Published online 00 Month 2021 in Wiley Online Library (wileyonlinelibrary.com).

becoming less true with the surgical advances afforded by micro-incisional vitrectomy surgery [Sommerville, 2015; Milston et al., 2016; Zeydanli et al., 2020].

Clinical inspection through the slit lamp of vitreous of patients presenting with SVO is often unrevealing, although advances in OCT and B-scan ultrasonography are enabling the presence, position, and severity of degenerative changes of the vitreous to be quantified more robustly [Mamou et al., 2015]. Because of the traditional downplaying of the effects of SVO, the lack of a clearly quantifiable disease, and the historically limited options for treatment, the symptomatic patient has all too often been dismissed by the ophthalmic profession and informed that they must adapt to life with their condition or advised that their symptoms will improve through a combination of acceptance, adaptation, and/or movement of the opacity away from the visual axis. Over the last decade or two, the attitude of the ophthalmic community to patients with SVO has altered somewhat. This shift in attitude is explained by the significant advances in vitreo-retinal surgical tools and techniques over the same time period, which now permit effective and safer removal of the vitreous and any opacities therein [Ivanova et al., 2016; Luff and O'Donnell, 2018] and by an increased appreciation of the effect that vitreous opacity can have on the quality of vision beyond that of visual acuity alone. Efforts have been made to understand the scattering effects that vitreous opacity has on the vision of the sufferer, with contrast sensitivity function (CSF) [Pelli and Bex, 2013] being one measure employed to evaluate the degradation in vision caused by SVO [Garcia et al., 2016]. Importantly, reduction in contrast sensitivity has been correlated with the presence of SVO and has been used as a quantitative index for determining the appropriateness of potential surgical intervention [Mamou, 2015; Garcia, 2016; Milston, 2016; Sebag, 2020, 2014]. However, contrast sensitivity testing is not standardised or regularly used in clinical evaluation.

To understand why it is that some patients with SVO present with severe symptoms, the scattering mechanisms of visible light, ~380–740 nm in free space (280–550 nm in the vitreous gel), by opacities suspended within the vitreous cavity need to be considered quantitatively. While there is much published work on electromagnetic scattering in other biomedical fields [Lin and Guy, 1974; Kim and Lin, 1998], there is, to date, very scarce representation of the effects of scattering by opacity within the vitreous in the literature [Serpetopoulos and Korakitis, 1998]. The vitreous consists of a meshwork of ultrafine collagen fibrils, 10–25 nm in diameter, that are prevented from coalescing by macro-molecules maintaining the spacing of the fibrils within the meshwork [Sebag, 1989]. Because the fibrils are much smaller (<1/10 th) than the wavelength of visible light in the vitreous media, they do not scatter visible light as they form a composite medium with mostly water, which can be effectively described by a single refractive index [Rytov, 1956], i.e. that of vitreous, ~1.335, in humans [Palanker, 2013]. In this case vitreous is transparent and optically homogenous, allowing light to propagate without scattering from lens to retina. However, degenerative processes due to ageing, disease, inflammation, and trauma can result in the breakdown of vitreous structure and the aggregation of the fine collagen fibrils, increasing their size until electromagnetic homogeneity is no longer an accurate description of the medium at optical wavelengths, with localised areas of liquefaction and expelled collagen clumping at significantly greater-than-wavelength dimensions. When this occurs, the vitreous becomes electromagnetically heterogenous and scattering of visible light occurs at the resulting discontinuities in refractive index, so that visible light no longer propagates undisturbed from lens to retina. Aggregations of type II collagen, which has a complex refractive index of ~$1.49 + i\ 0.001$ [Sekar et al., 2017; Scholkmann et al., 2014; Sekar et al., 2017], are suspended in aqueous humour, refractive index ~1.3335 [Palanker, 2013], and result in scattering through refraction and diffraction of incident optical energy. It should be noted that because of the very small extinction coefficient of collagen (10^{-3}), very little optical energy will be absorbed by the opacity and hence visual effects are almost entirely due to the forward redistribution (scattering) of incident light. Although the word “opacity” is used medically, this is rather misleading as the material causing the visual effects may be transparent, the visual effects arising from interference caused by differences in refractive indices between the “opacity” and the surrounding vitreous. The authors' aims are to prove, theoretically, that vitreous opacity can result in variations in the intensity distribution on the retina, and thus be perceived by the patient with SVO; to show that backscattering from vitreous opacity is very much smaller than forward scattering and therefore explain the difficulty in matching subjective symptoms with objective examination; and to explain the link between degradation in contrast sensitivity function with the presence of SVO. In providing this solid scientific explanation, based on physics, the authors hope to provide explanation and additional reassurance to clinicians considering surgical intervention for SVO in an eye with unremarkable clinical examination.

MATHEMATICAL MODEL

The authors use a Fourier optics model of a simplified human eye together with a mathematical model of human vision implemented in the commercial software MATLAB (MathsWorks, Natick, MA). The optical model is based on the solution of the Helmholtz equation [Goodman, 1996; Yariv, 1997; Mezouari and Harvey, 2003] in the paraxial limit and we confine our interest to two dimensions for computational speed. The paraxial limit is an excellent approximation in the case of the human eye since the F-number of the human eye is approximately between two and eight depending on the pupil diameter, giving angular deviations from the visual axis of between 4° and 14°, which are very well approximated paraxially. Vitreous opacity, which acts as the scattering object, is represented by the complex reflection and transmission coefficients of a single planar dielectric layer [Kapilevich et al., 2014]. In the model, the opacity is completely specified by the complex refractive index, $n' + in''$, of the opacity; the axial thickness and width of this layer; the refractive index of the surrounding medium, n_a (the vitreous); the incident spectrum of light, here assumed white; the distance from scattering object to the retina; and the focal length of the cornea/lens optical system. See Figure 1 for a diagram of the model eye used. It should be noted that any model depending on exact electromagnetic solutions is unrealistic for this problem because of the widely variable form that vitreous opacity may take. Here, the aim is to estimate the magnitude of visual effects and explain the main clinical observations for SVO, which are: Why it is that vitreous opacity can result in severe symptoms to those afflicted, but the vitreous is often unremarkable upon clinical examination? What are the key parameters that determine the optical effect of vitreous opacity (i.e. pupil diameter, opacity size, position of opacity relative to retina)? Does SVO degrade CSF? And is this degradation correlated to other symptoms of SVO?

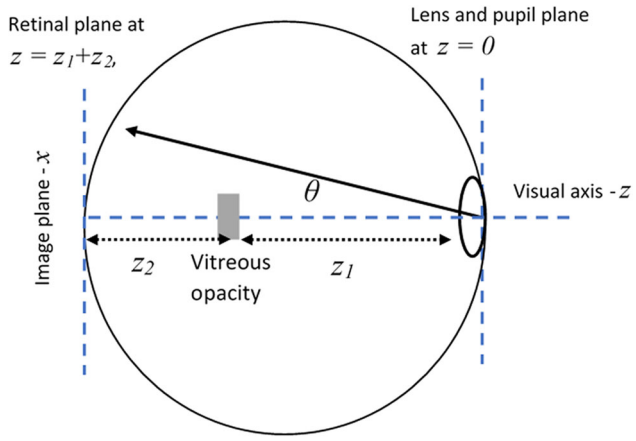

Fig. 1. Simplified human eye model, giving the definition of the angle used in plots throughout this article. The axial length of the human eye, the distance from the front of lens to the retina $z_t = z_1 + z_2$, is assumed to be 22.3 mm in this article [Bhardwaj and Gandhi Rajeshbhai, 2013].

The model uses the paraxial solutions of the Helmholtz equation, Equation (1),

$$\nabla^2 E + k_0^2 n^2 E = 0 \tag{1}$$

where E is the electric field, $k_0 = \frac{2\pi}{\lambda}$is the wavenumber in free space, λ is the wavelength in free space, and n is the refractive index of the medium in which the wave is propagating; there are two different media in the model: the vitreous has refractive index n_a and the opacity refractive index n_b. We develop a two-dimensional model using z to represent distance along the visual axis and x to represent displacement on the retinal plane (see Fig. 1). The general solution to Equation (1) in two dimensions is,

$$E(x, z) = \int_{-\infty}^{\infty} F(k_x) e^{i(k_x x + k_z z)} dk_x \tag{2}$$

where $k_0^2 n^2 = k^2 = k_x^2 + k_z^2$ and $k_x$and k_y are the lateral and axial wavenumber components, respectively. Using the paraxial approximation, $|k_x| << |k|$, we have $k_z \approx k - \frac{k_x^2}{2k}$; applying this result to Equation (2), the paraxial electric field distribution is well approximated by,

$$E(x, z) = e^{ikz} \int_{-\infty}^{\infty} F(k_x) e^{-i\frac{k_x^2 z}{2k}} e^{ik_x x} dk_x \tag{3}$$

Equation (3) can be written as an inverse Fourier transform,

$$E(x, z) = e^{ikz} \mathfrak{I}^{-1}\left\{ F(k_x) e^{-i\frac{k_x^2 z}{2k}} \right\} \tag{4}$$

where $\mathfrak{I}^{-1}\{A(k_x)\} = \int_{-\infty}^{\infty} A(k_x) e^{ik_x x} dk_x$. Equation (4) provides an expression for $F(k_x)$ in terms of the "input field distribution," $E(x, 0)$, which is the field distribution at the plane $z = 0$; hence, we have the Fourier transform of the input field distribution as Equation (5),

$$F(k_x) = \mathfrak{I}\{E(x, 0)\} \tag{5}$$

where $\mathfrak{I}\{a(x)\} = \frac{1}{2\pi}\int_{-\infty}^{\infty} a(x) e^{-ik_x x} dx$. Now, we may write Equation (4) as,

$$E(x, z) = e^{ikz} \mathfrak{I}^{-1}\left\{ \mathfrak{I}\{E(x, 0)\} e^{-i\frac{k_x^2 z}{2k}} \right\} \tag{6}$$

Utilising the convolution theorem, we may write Equation (6) as,

$$E(x,z) = \frac{e^{ikz}}{2\pi} E(x,0) \otimes \Im^{-1}\left\{ e^{-i\frac{k_x^2 z}{2k}} \right\} \tag{7}$$

where $\otimes$ represents the one-dimensional spatial convolution operation.

Since $\Im^{-1}\left\{ e^{-i\frac{k_x^2 z}{2k}} \right\} = \sqrt{\frac{2\pi k}{iz}}\, e^{i\frac{kx^2}{2z}}$, then Equation (7) can be written as,

$$E(x,z) = e^{ikz} \sqrt{\frac{k}{i2\pi z}}\, E(x,0) \otimes D(x,z) \tag{8}$$

where $D(x,z) = e^{i\frac{kx^2}{2z}}$. Equation (8) provides a prescription for propagating a field distribution from the plane $z = 0$ to the plane z. At the eye's pupil the input field is given by the plane wave,$A(x) = e^{ik_0 x n_a \sin\theta}$, where, for simplicity, we have assumed an amplitude of unity and that the eye is receiving light from a point source located at infinity. Within the eye, the spherical wave propagates at angle of θ to the visual axis (z-axis). This field distribution is multiplied by the pupil function, $P(x)$, defined to be unity within the pupil (radius a) and zero outside and then multiplied again by the thin lens function, $L(x) = e^{-i\frac{kx^2}{2f}}$, where $k = k_0 n_a$. This function focuses the incident wave to a minimum beam width at the focal distance f from the lens. Hence the field distribution immediately after the pupil and lens is given by,

$$\begin{aligned} E(x,0) &= P(x)A(x)L(x) \\ &= \begin{cases} e^{ik\left(x\sin\theta - \frac{x^2}{2f}\right)}\,; & |x| \le a \\ 0\,; & |x| > a \end{cases} \end{aligned} \tag{9}$$

This input field is then propagated from the pupil ($z = 0$) to the opacity plane ($z = z_1$) using Equation (8),

$$E(x,z) = e^{ikz_1} \sqrt{\frac{k}{i2\pi z_1}}\, (P(x)A(x)L(x)) \otimes D(x,z_1) \tag{10}$$

At the opacity plane, the incident field is partially reflected from the opacity and partially transmitted through the opacity; the forward and back scattered fields are obtained by multiplying the field distribution given by Equation (10) by further scattering function in the opacity plane. The scattering function is given by R (Equation 11) for back scattering and T (Equation 12) for forward scattering,

$$R = \begin{cases} \frac{r(1 - e^{i2k_0 n_b h})}{1 - r^2 e^{i2k_0 n_b h}}; & |x| < a \\ 0\,; \quad |x| \ge a \end{cases} \tag{11}$$

$$T = \begin{cases} \frac{(1 - r^2) e^{ik_0 n_b h}}{1 - r^2 e^{i2k_0 n_b h}}; & |x| < a \\ 1 \qquad\quad ; & |x| \ge a \end{cases} \tag{12}$$

where a is the pupil radius, $r = \frac{n_a - n_b}{n_a + n_b}$, and h is the thickness of the opacity. Equations (11) and (12) are obtained by considering the reflection and transmission of electromagnetic waves by a planar layer through applying appropriate electromagnetic boundary conditions [Kapilevich et al., 2014].

One should note that the refractive index of the opacity may be a complex number, that is there is a refractive index, n_b', and extinction coefficient, n_b'', which together constitute the complex refractive index, $n_b = n_b' + i n_b''$. It is assumed that healthy vitreous is lossless and therefore has zero extinction coefficient. From Equations (10) and (12) the field distribution after the opacity is given by,

$$\begin{aligned} E(x,z_1) = e^{ikz_1} \sqrt{\frac{k}{i2\pi z_1}}\, ((P(x)A(x)L(x)) \\ \otimes D(x,z_1))T(x) \end{aligned} \tag{13}$$

And from Equations (10) and (11) the field distribution reflected by the opacity is given by,

$$\begin{aligned} E(x,z_1) = e^{ikz_1} \sqrt{\frac{k}{i2\pi z_1}}\, ((P(x)A(x)L(x)) \\ \otimes D(x,z_1))R(x) \end{aligned} \tag{14}$$

Finally, the field distribution on the $z = h_1 + h_2$ plane is obtained by taking Equation (13) as the input field distribution and appropriately applying Equation (8), to give the forward scattered field, E_F, on the retinal plane.

$$\begin{aligned} E_F(x) = E(x,z_2) = e^{ik(z_1+z_2)} \frac{k}{i2\pi\sqrt{z_1 z_2}} \\ (((P(x)A(x)L(x)) \otimes D(x,z_1))T(x)) \otimes D(x,z_2) \end{aligned} \tag{15}$$

Similarly, for the field back scattered at the lens plane ($z = 0$), E_B,

$$E_B(x) = E(x,0) = e^{ik2z_1}\frac{k}{i2\pi z_1}(((P(x)A(x)L(x)) \otimes D(x,z_1))R(x)) \otimes D(x,z_1) \quad (16)$$

The point spread function (PSF) at the retinal and lens planes are obtained by taking the modulus square of Equations (15) and (16) respectively, i.e. $PSF(x) = |E(x)|^2$. It should be noted that the PSF in this model is not isoplanatic, since Equations (15) and (16) depend on whether the light passed through the opacity is determined by the angle of propagation θ and if so, where it has passed through the opacity.

From the PSF, Equation (15), the modulation transfer function (MTF) is obtained by,

$$MTF(\gamma) = |\Im\{PSF(x)\}| \quad (17)$$

The MTF is a measure of how spatial frequencies are filtered when passed through an optical system and are conventionally plotted as a function of angle, θ, (degrees) versus spatial frequency, μ, in units of cycles per degree (cpd). Conversion from x-coordinate in the retinal plane to θ-coordinate is realised by $x = \frac{\pi z_t}{180}\theta$ and conversion from spatial frequency in radians per metre, γ, to spatial frequency in cycles per degree, μ, is realised by $\mu = \frac{z_t}{360 n_a}\gamma$, where $z_t = z_1 + z_2$.

The model computes values over ten equally spaced wavelength steps, from 380 to 740 nm in free space, with each wavelength step having the same intensity (white light). The light is assumed temporally incoherent and accordingly intensities are summed over each wavelength step; thus the PSF is formed by adding the intensities of the 10-point spread functions calculated for each wavelength step. However, less significant wavelength-dependent effects, such as dispersion in the vitreous and opacity, are not included as these effects are likely to be very small over the visible band. The spatial resolution of the model is set at $\lambda/10$ of the shortest wavelength of light used in the simulations, giving a value of 38 nm, thus ensuring that interference effects are accurately computed. Note, all equations given are valid for continuous distributions and since MATLAB operates discretely, integrals in equations are replaced with the appropriate summations when implemented in code.

Equation (17) provides the MTF at the surface of the retina and does not include the modulation effects of the retina, optic nerve, and brain. These effects are highly important as human vision has a peak spatial frequency sensitivity around a few cycles per degree [Lesmes et al., 2010] and a rapid tail-off at higher spatial frequencies that is a consequence of cone cell size and density and neuro modulation effects and is not explained by the optical physics of the eye. Mathematical models of human vision are numerous, with a comprehensive description of various models provided in Watson and Ahumada [2005]. The authors have chosen, somewhat arbitrarily, to use an asymmetric parabolic function in log-log space as there is best fit numerical data of "normal" human vision provided for this model [Chung and Legge, 2016]. The MTF on the retina is calculated using Equation (17) and the mathematical model of human vision is given by the contrast sensitivity function, CSF. The contrast sensitivity is linked to the optical MTF of Equation (17) by assuming the presence of an additional neural MTF term, MTF_{Neural}, which characterises spatial filtering from the retina to the brain, Equation (18)

$$CSF = |MTF_{Optical} MTF_{Neural}| \quad (18)$$

With,

$$\log_{10}(CSF') = \begin{cases} \alpha - \beta^2(\log_{10}(\mu) - \log_{10}(\mu_P))^2 & \mu < \mu_P \\ \alpha - \delta^2(\log_{10}(\mu) - \log_{10}(\mu_P))^2 & \mu \geq \mu_P \end{cases} \quad (19)$$

where α, β, and δ are constants and μ and μ_P are the spatial frequency in cycles per degree and spatial frequency at which the CSF is maximum respectively. The values used in Equation (19) are those that gave best fit with normal human vision [Chung and Legge, 2016]: $\alpha = 2.22$, $\beta = 0.68$, $\delta = 1.28$, and $\mu_P = 2.5$. Note that CSF is used in vision science to measure the sensitivity of the visual system as a function of spatial frequency [Pappas et al., 2005; Pelli and Bex, 2013]. We assume, as no specific information was given, that the best fit data obtained were measured for pupils of 4 mm diameter in eyes without vitreous opacity and that this gives a contrast sensitivity function CSF'. This assumption does not significantly affect the following results if it is altered to 2 mm or 8 mm, which mark the extreme values for the human eye. Using Equation (18) we have,

$$CSF' = |MTF'_{Optical} MTF|_{Neural} \quad (20)$$

From Equations (18) and (20) and assuming that the neural MTF is independent of pupil diameter, we

can compute the CSF of an eye with opacity and a different pupil diameter according to Equation (21)

$$CSF = \left| \frac{MTF_{Optical}}{MTF'_{Optical}} \right| CSF' \qquad (21)$$

In the calculations presented, the value of CSF' is normalised to have a maximum value of unity, which occurs at spatial frequency $\mu_P = 2.5$cpd. $MTF'_{Optical}$ is the MTF calculated by Equation (17) for an eye with 4 mm diameter pupil and in the absence of opacity. In the model, the MTF and CSF step size is 0.0474 cpd. Variations in CSF from eye to eye will have some effect on the results predicted by application of Equation (21); however, the authors do not have information on the variance of parameters α, β, δ, and μ_P that would enable such variations in CSF to be explored. Therefore, predicted results are for average human vision. The MATLAB code can be summarised as taking an incident planar wave and focusing this through a refractive optical system of focal length *f*. The amplitude distribution is then propagated to the plane in which the opacity is located, Equation (10), where the Fresnel reflection and transmission coefficients, Equations (11) and (12) respectively, are applied to calculate the forward and backscattered amplitudes. These amplitudes are then propagated onto the retina and lens planes, Equations (15) and (16) respectively, to give the amplitude distributions which are used to calculate the effects of vitreous opacity.

SIMULATION RESULTS

Quantifying the Effect of Vitreous Opacity on Vision

Modelling using the MATLAB code developed by the authors allows the computation of PSF, the spatial frequency domain analogue, MTF at the retina, and the CSF for the whole human visual system to be estimated. The computed PSF, Equation (15), is normalised so that it has maximum value of unity in the case of no vitreous opacity; this is done so that comparison may be made of the effect on forward scattered intensity by the presence of vitreous opacity. The MTF, Equation (17), is conventionally scaled, so that it has a value of unity at zero spatial frequency.

Even with the simplified human eye model presented, there are issues with fully exploring the multivariate space of the model simulations. To reduce complexity, some parameters of the model are fixed with appropriate values. The fixed parameters are the axial length of the eye (22.3 mm) and the focal length of the eye (also 22.3 mm), which is equal to the axial length for an emmetropic eye and the angle at which the light propagates through the eye, which is chosen to be along the visual axis ($\theta = 0$). Note, since in the simplified mathematical model of the eye used, all refraction occurs at the front surface of the eye and so the axial length and not the depth of the vitreous cavity is the important parameter. With these fixed parameters, the variables are limited to the distance of the opacity from the retinal plane, the thickness and width of the vitreous opacity, and the pupil diameter. Further, by equating the opacity thickness and width to form a single variable of opacity "size," the model is reduced to a manageable three degrees of freedom, suitable for brief exploration and discussion in a single article.

Figures 2 and 3 display the computed PSF, MTF, and CSF for an eye with no opacity and a 25 μm size opacity, located 2 mm from the retina, respectively. The effect of the centrally located vitreous opacity is clear, with the greatest effect presenting for the smallest pupil diameter. The opacity results in the central maximum intensity of the PSF decreasing and the intensity of the side lobes (the oscillations that occur outside of the central maxima of the PSF) increasing. The physical explanation for these effects on the PSF is simply that the opacity redistributes (scatters) the light in a forward direction with the optical energy being deflected though larger angles, increasing the intensity in the side lobes and a consequent reduction of intensity in the central maxima. When examined in spatial frequency space, the MTF is reduced in the spatial frequency range up to about 50 cpd, with significant reduction up to about 30 cpd, while being largely unaffected at much higher spatial frequencies. The very high spatial frequency components present in the MTF are not present in human vision due, predominantly, to the finite sampling size of cone cells in the retina, with cone cell density being maximum in the foveal region with a spacing of ~2.7 μm [Wells-Gray et al., 2016]. This cut-off effect is clearly seen in the CSF plots in Figures 2 and 3, with CSF falling to about 1% of peak value at 30 cpd.

The reduction in the maximum intensity of the central PSF maxima caused by the presence of vitreous opacity can be usefully quantified by defining the reduction in relative intensity (RRI), which is expressed as a percentage decrease of the intensity without opacity, Equation (22).

$$RRI = 100\left(\frac{\max(PSF) - \max(PSF_{opacity})}{\max(PSF)}\right) \qquad (22)$$

where PSF is the PSF with no opacity, $PSF_{opacity}$ is the PSF with opacity, and *max* requires taking the global maximum value of that function.

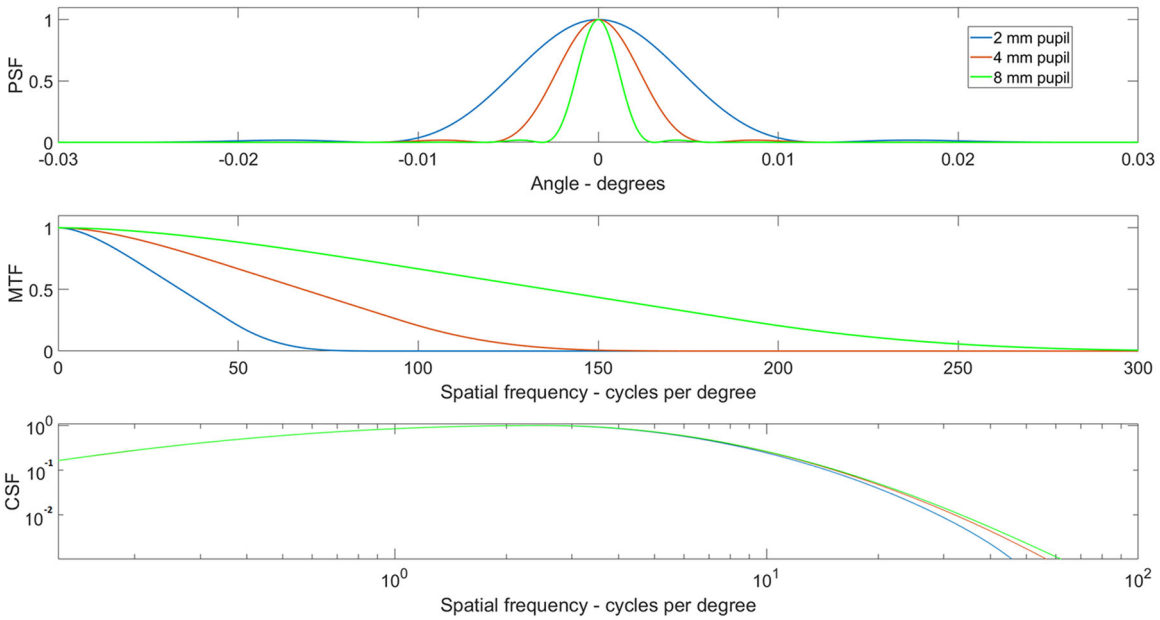

Fig. 2. The point spread function, modulation transfer function, and contrast sensitivity function predicted by the model for an emmetropic human eye with no vitreous opacity and with different pupil diameters. The point spread function and modulation transfer function are determined by the optical properties of the eye anatomy and are representative of effects at the retinal surface, whereas the contrast sensitivity function is calculated from measurements made on the complete human vision system and is representative of what is perceived. The contrast sensitivity function is plotted in log-log format as is conventional in vision science.

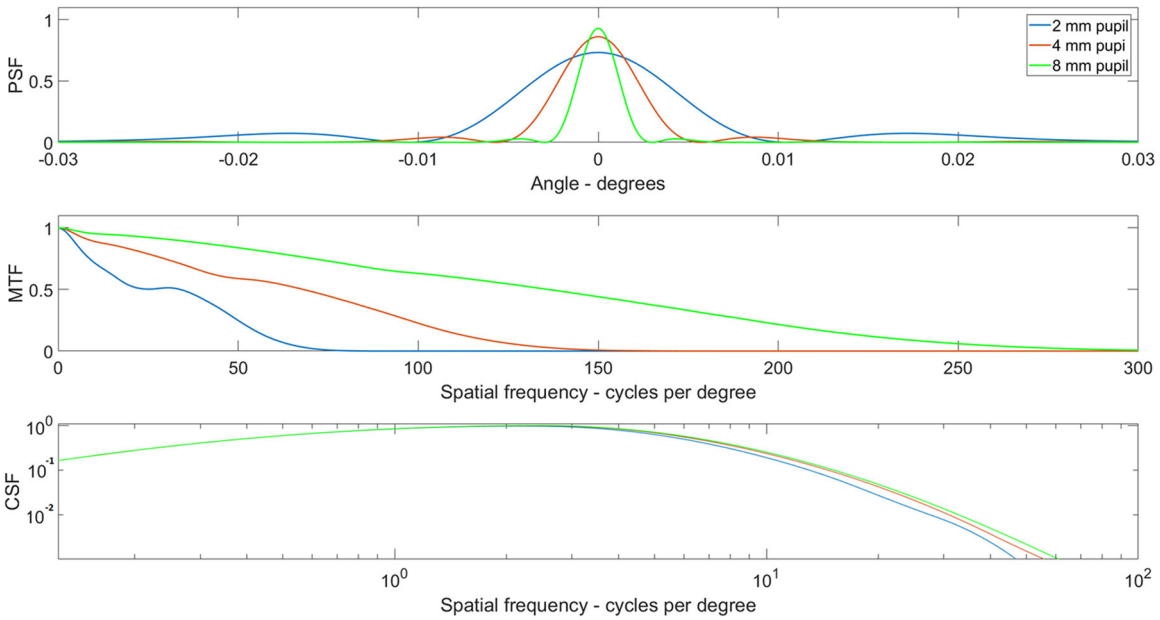

Fig. 3. The point spread function, modulation transfer function, and contrast sensitivity function predicted by the model for an emmetropic human eye with a 25 µm collagen vitreous opacity located 2 mm from the retinal plane. The opacity is located symmetrically on the visual axis. The effects of the vitreous opacity are clearly seen in the point spread function, modulation transfer function, and contrast sensitivity function plots, with greatest effect occurring for the smallest pupil diameter. The contrast sensitivity is plotted in log-log format as is conventional in vision science.

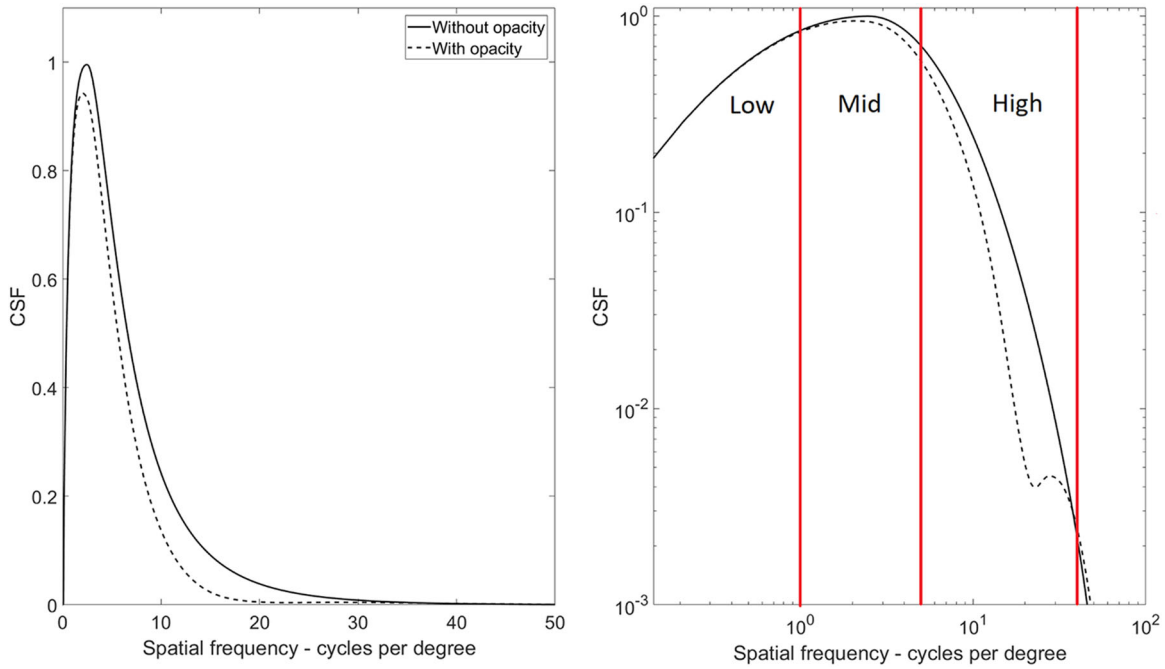

Fig. 4. The difference between two contrast sensitivity functions, with and without vitreous opacity and the definitions of low, mid, and high spatial frequency used to quantify the effect of vitreous opacity on contrast sensitivity function. An eye with a 2 mm pupil dimeter and with 50 µm vitreous opacity located 2 mm from the retina is modeled. The plots are given in linear space (left) and log-log space (right).

The RRI is used here as the principal measure of the severity of vitreous opacity because decrease in intensity caused by vitreous opacity results in localised shadowing on the retina when a constant brightness background, such as a blue sky or white light computer monitor, is viewed. The RRI, Equation (22), gives a direct measure of the maximum localised reduction in intensity produced by the presence of vitreous opacity. However, opacity also scatters incident light to wider angles and so a measure of the effect on overall vision (CSF) by vitreous opacity is also required. To quantify the degradation in CSF caused by vitreous opacity, the difference between CSF with and without vitreous opacity is computed and divided by the CSF without vitreous opacity, Equation (23), to give the decrease in CSF as a percentage. These values are averaged over three spatial frequency ranges: low, mid, and high, corresponding to spatial frequency ranges of 0.1–1, 1–5, and 5–40 cpd, respectively, so that the effect of degradation of CSF due to vitreous opacity can be quantified broadly by spatial frequency range. See Figure 4 for illustration.

$$\Delta CSF\% = 100\left(\frac{CSF - CSF_{opacity}}{CSF}\right) \qquad (23)$$

where CSF is the CSF with no opacity, $CSF_{opacity}$ is the CSF with opacity, and the mean value of $\Delta CSF\%$ is taken over the chosen spatial frequency ranges.

Finally, we also wish to compare the effect of opacity on the intensity distribution on the retina as a ratio to the reflected or backscattered intensity distribution at the pupil plane, which is available for clinical viewing. A ratio of the change in central intensity on the retinal plane produced by opacity to the maximum backscattered intensity on the pupil plane gives a useful measure of the predicted anisotropy in forward and back scattering. The forward to back scattering ratio FBR is given in Equation (24)

$$FBR = \frac{\max(PSF) - \max(PSF_{opacity})}{\max(PSF_B)} \qquad (24)$$

where PSF_B is the backscattered intensity distribution obtained from taking the square of the modulus of Equation (16). The FBR is large and is better expressed as a decibel quantity, $dB_{FBR} = 10\log_{10}(FBR)$.

The described model was run over a range of pupil diameters of 2, 4, and 8 mm, which cover the usual range of the human eye [Watson and Yellott, 2012]; a range of opacity sizes, from 10 µm through to 96 in 5 µm steps; and a range of opacity separations

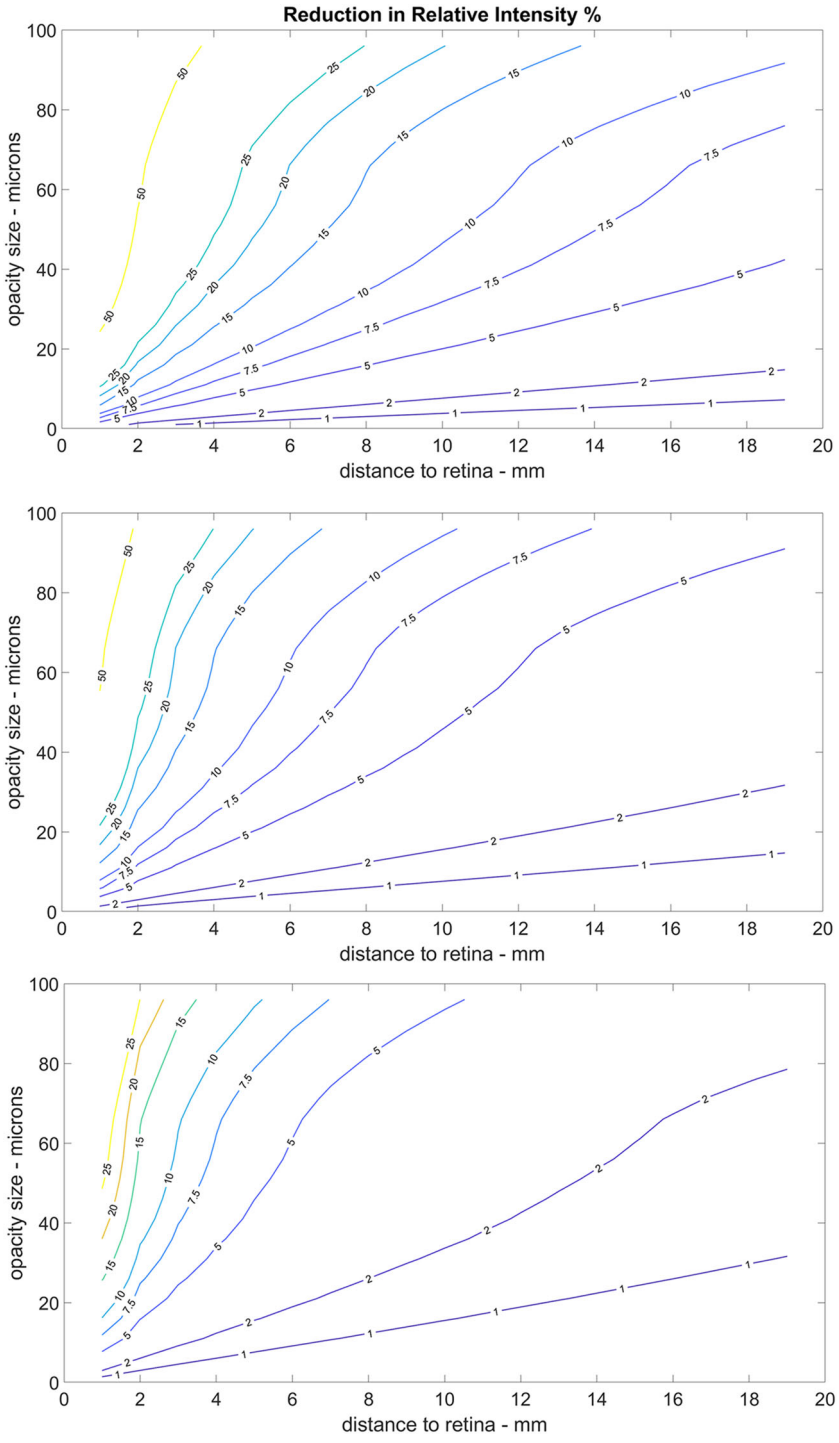

Fig. 5. Contour plot of reduction in relative intensity (RRI) caused by opacity of different sizes and at different distances to the retinal plane for an eye with three different pupil diameters. 2 mm (top plot), 4 mm (middle plot), and 8 mm pupil (bottom plot). The values given on the contours are the RRI as a percentage.

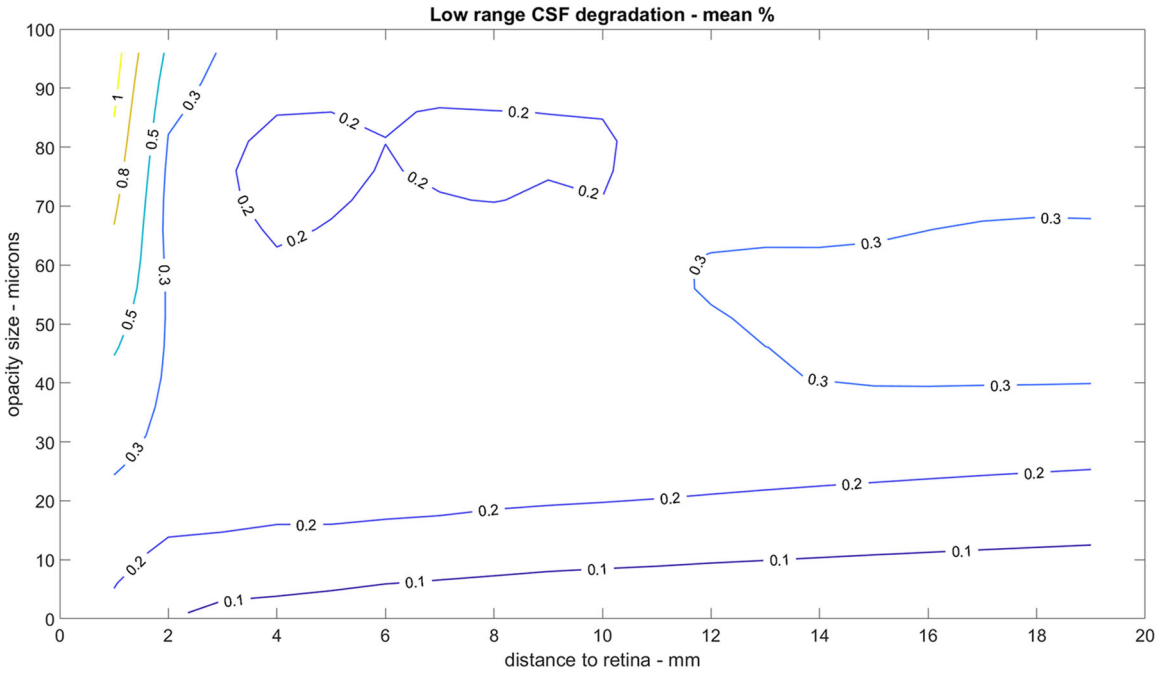

Fig. 6. Contour plot of mean decrease in contrast sensitivity function in the low spatial frequency range caused by opacity of different sizes and at different distances to the retinal plane for an eye with a 2 mm pupil diameter. The values given on the contours are in percent.

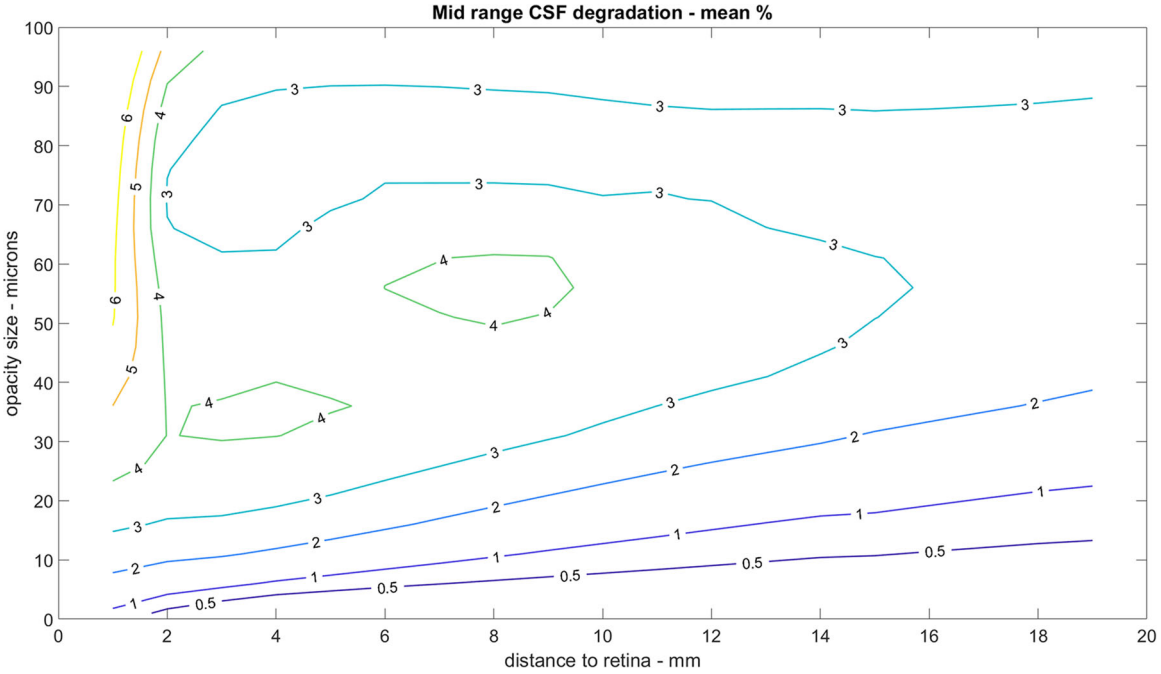

Fig. 7. Contour plot of mean decrease in contrast sensitivity function in the mid spatial frequency range caused by opacity of different sizes and at different distances to the retinal plane for an eye with a 2 mm pupil diameter. The values given on the contours are in percent.

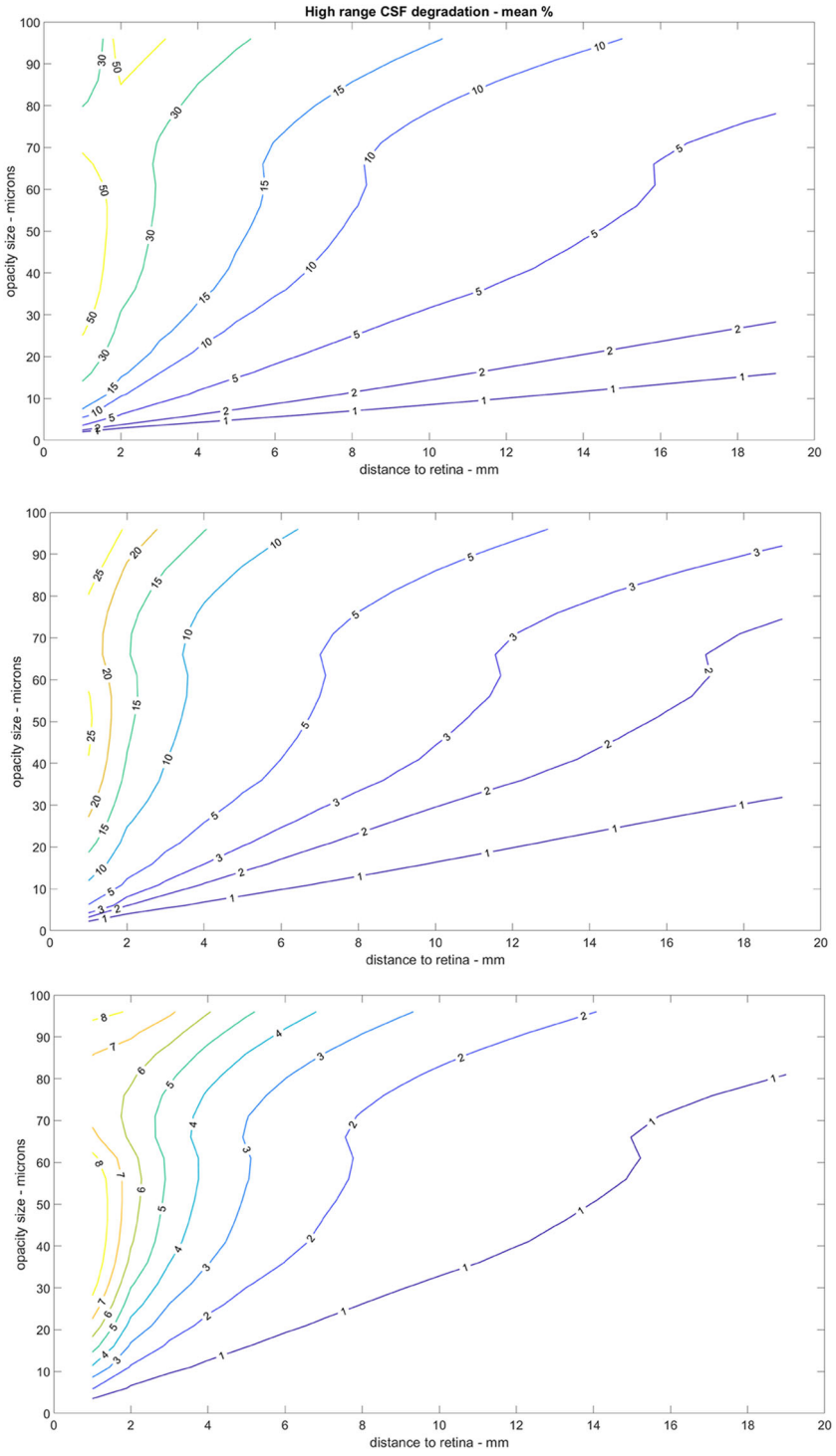

Fig. 8. Contour plot of mean decrease in contrast sensitivity function in the high spatial frequency range caused by opacity of different sizes and at different distances to the retinal plane for an eye with three different pupil diameters. 2 mm (top plot), 4 mm (middle plot), and 8 mm pupil (bottom plot). The values given on the contours are in percent.

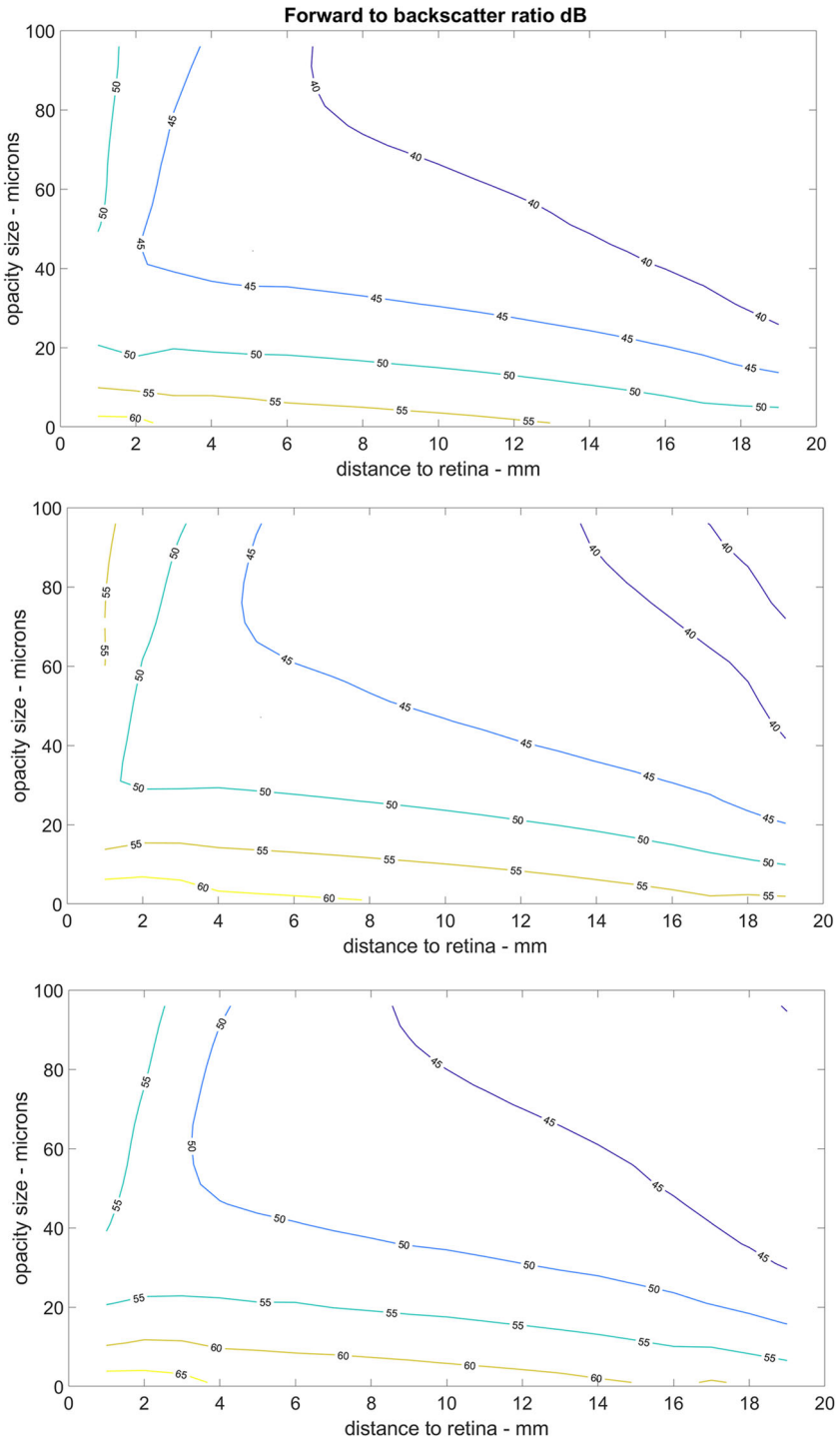

Fig. 9. Contour plot of forward to backscatter ratio from opacity of different sizes and at different distances to the retinal plane for an eye with three different pupil diameters. 2 mm (top plot), 4 mm (middle plot), and 8 mm pupil (bottom plot). The values given on the contours are the FBR in dB.

TABLE 1. Correlation Coefficients Between RRI and Mean CSF Degradation at the Three Chosen Spatial Frequency Ranges

Spatial frequency range pupil diameter mm	Low	Mid	High
	0.1–1 cpd	1–5 cpd	5–40 cpd
2	0.646 to 0.748	0.643 to 0.747	**0.832–0.884**
3	0.357 to 0.519	0.338 to 0.503	**0.971–0.980**
4	0.014 to 0.212	0.130 to 0.321	**0.973–0.982**
5	−0.093 to 0.109	0.047 to 0.244	**0.950–0.967**
6	−0.173 to 0.027	0 to 0.198	**0.921–0.946**
7	−0.208 to −0.01	−0.028 to 0.172	**0.897–0.930**
8	−0.207 to 0	−0.049 to 0.152	**0.877–0.916**

Note: The correlation coefficients listed are the ranges for 95% confidence. A value of 0 represents no correlation, while a value of 1 indicates perfect positive correlation and a value of −1 perfect negative correlation. Values above 0.8 are highlighted in bold.

from the retinal plane, from 1 mm through to 19 mm in 1 mm steps. The RRI, Equation (18), contrast degradation, Equation (23), and FBR, Equation (24) were computed for each of these $3 \times 19 \times 20 = 1140$ scenarios, and then these data were plotted as contour plots to show the dependence of these three measures on the variables of pupil diameter, opacity size, and distance of opacity from the retinal plane; see Figures 5-9.

Although the collagen opacity absorbs almost none of the optical energy incident upon it (i.e. it is nearly transparent), there is still a significant optical effect at the retinal plane. Figure 5 shows that shadowing, resulting from reduced intensity from the opacity as compared to no opacity, can be considerable and that this effect is strongly dependent on opacity size and the distance of the opacity from the retinal plane. For a constant opacity size, the RRI falls off rapidly with increasing distance from the retinal plane, making the visual effects of SVO decrease with increasing distance from the retina. As expected, for constant distance from the retinal plane, increasing opacity size results in increasing RRI, and so larger opacity results in greater visual effects. The pupil size strongly influences the effects of vitreous opacity, with smaller pupil diameters giving greater RRI for the same values of retinal separation and opacity size.

Figures 6-8 display the mean degradation in CSF. Importantly, the degradation of CSF is predicted to be spatial frequency-dependent, with quite different trends being apparent for low, mid, and high spatial frequency regions; compare Figure 6 and Figure 7 with Figure 8. For the 2 mm diameter pupil, the greatest degradation in CSF is to be found in the high spatial frequency region, with values ~50% being reached for opacity close to the retina, whereas in the mid-spatial and low spatial frequency regions these values only reach ~6% and ~1%, respectively. The CSF in the high spatial frequency ranges, Figure 8, are very similar in shape to the corresponding RRI plots, Figure 5, whereas the plots for low and mid spatial frequency CSF degradation, Figures 6 and 7, look quite different. This similarity can be quantified by calculating the 95% confidence correlation values between RRI and CSF degradation; the results are tabulated in Table 1. The correlation between the principal symptom of vitreous opacity, quantified by RRI, and degradation of CSF is very strong for the high spatial frequency region, but is weak or uncorrelated for the low and mid-spatial frequency regions. Smaller diameter pupils (2 and 3 mm) display some degree of correlation in the mid and low spatial frequency regions, but this vanishes for pupil diameters of 4 mm and larger. The close similarity of degradation of CSF with RRI is to be expected from the principle of conservation of energy, with virtually no absorption of optical energy within the opacity and extremely low backscattering; the reduction in intensity of the central PSF maxima produced by the opacity must be balanced by increased intensity in the PSF side-lobes, leading to degradation of CSF. What is less obvious is that the frequency dependence of this degradation should be greater in the high spatial frequency range, and symptoms of shadowing caused by vitreous opacity should correlate strongly only to degradation in high frequency CSF. To our knowledge, these predictions, founded on the physics of electromagnetic scattering, are unique in the literature, and further work could be undertaken to investigate clinically whether the predicted magnitudes of CSF diminution and the correlation between floater severity and degradation of high frequency (5–40 cpd) CSF is observed in practice.

Finally, Figure 9 depicts the forward to back scatter ratio; there is a huge difference between the maximum change in the forward scattered intensity with and without opacity to the maximum back scattered intensity with opacity. Values above 40 dB

and reaching 65 dB are predicted, corresponding to FBR values of between approximately 10^4 and 10^6. The very large asymmetry between reflected intensity and variations in forward scattered intensity is of significance as it is consistent with the sometimes-noted difficulty in observing vitreous opacity on clinical examinations at the slit lamp. The predictions are also suggestive that absence of such clinical observation can in no way be taken as a guarantee that the patient cannot observe significant effects when "looking through" vitreous opacity.

CONCLUSIONS

Vitreous opacity is a common clinical presentation to optometrists and ophthalmologists. In some cases, sudden onset of floaters can be a sign of retinal tear following acute posterior vitreous detachment and other potentially vision-threatening retinal pathologies. However, persistent vitreous opacity in the absence of retinal pathology is common and in a small but significant population can cause visual dysfunction and a reduction in quality of life. The simplified human eye model described here and computationally implemented offers a physical explanation as to the significant visual effects that are reported by a small, but significant, subset of those with SVO; explains why clinical observation with slit lamp alone is an unreliable diagnostic tool for SVO; theoretically links degradation of CSF with the presence of SVO; and demonstrates that degradation of CSF in the spatial frequency range 5–40 cpd is very strongly correlated to the degree of shadowing caused by vitreous opacity.

The model implemented accounts for common symptoms of SVO, i.e. the perception of well-defined shadowing (RRI) in the visual field (see Fig. 5), with patients often reporting dark shapes that move through their visual field on eye movement. The severity of this shadowing is dependent on both the size of the opacity and the distance that the opacity is located from the retina. Not surprisingly, larger opacity results in greater shadowing (this effect will be both in depth of shadowing and also in the perceived angular size of the floater). Opacity suspended closer to the retina produces greater shadowing effects than the same opacity located further from the retina. However, opacity that is closer will produce shadowing with smaller angular size than the same opacity located further away, so the expected results of opacity located close to the retina is a well-defined floater with significant shadowing effects, while opacity located further from the retina will produce a larger and more diffuse shadowing effect, perhaps perceived as more of a 'clouding' in vision. The improvement in symptoms for some patients complaining of SVO following posterior vitreous detachment may be explained by this effect as the vitreous opacity is moved further from the retina by the collapsing gel structure [Ivanova et al., 2016].

A significant prediction of the model is the very strong dependence on shadowing of pupil diameter. Narrow pupils give much greater effects than wider pupils. Thus, one would expect that SVO symptoms would become very noticeably worse in brightly lit environments, where light-induced miosis [Maqsood, 2017] would increase the depth of shadowing perceived by vitreous opacity, and this is indeed often reported [Luff and O'Donnell, 2018]. The effect also suggests that symptoms of SVO should be improved by mydriatic drugs, such as atropine eye drops, and, indeed, such an effect has been reported in the literature and used as a non-surgical treatment for SVO [Kaymak, 2017].

Degradation of contrast sensitivity function has been linked with SVO, and this is important since CSF can be measured clinically and thus could be used as a metric to indicate objectively that surgical intervention had made a measurable improvement. Currently, most surgical intervention for SVO is based entirely on the reported, and hence subjective, symptoms of the SVO patient and this lack of objective measure may deter surgeons from offering surgery to the SVO patient. By utilising a mathematical model of human vision, the optical predictions of the model presented here can be used to predict the effect of SVO on contrast sensitivity function. CSF is predicted to be degraded by SVO, with the greatest effects in the high spatial frequency range of 5–40 cpd. High spatial frequency CSF degradation shows the same trends as RRI: with greatest effect observed for large opacity, opacity that is close to the retina, and where the pupil diameter is smallest (see Fig. 8). The similarity of the trends of high-frequency CSF degradation and RRI is quantified by correlating these two measures; see Table 1. Since RRI is hard to measure directly, requiring the shadows cast due to vitreous opacity to be located and measured on the retina, correlation of this with a clinically measurable quantity is important. The very high degree of correlation between RRI and CSF suggests that degradation and subsequent post-surgical improvement in high frequency CSF may be a useful clinical metric for SVO.

Collagen has a small extinction coefficient and a refractive index which is not vastly different from vitreous, yet even 10-μm sized opacity composed of

this material is predicted to cause symptoms if the opacity is located close to the retina. While collagen aggregations are one likely cause of SVO, even the liquefaction of vitreous with corresponding small alterations in refractive index could give rise to symptoms. The term vitreous opacity is therefore somewhat of an inaccurate description, as symptoms may be produced by entirely transparent media that result in localised changes in refractive index. Although unlikely to be adopted, SVRI (Symptomatic Vitreous Refractive Inhomogeneities) is a more accurate acronym.

Backscattering by opacity is extremely low when compared to the variation in intensity caused on the retina by the opacity, with values of 10^4–10^6 predicted; see Figure 9. Perhaps one of the most significant problems of SVO is often the difficulty in matching reported symptoms with clinical examination. With the forward to backscatter ratios predicted by the model presented, it is apparent that unremarkable clinical examination is to be expected even in the presence of the most debilitating of symptoms.

REFERENCES

Bhardwaj V, Rajeshbhai GP. 2013. Axial length, anterior chamber depth—A study in different age groups and refractive errors. J Clin Diagn Res 7:2211–2212.

Chung ST, Legge GE. 2016. Comparing the shape of contrast sensitivity functions for normal and low vision. Invest Ophthalmol Vis Sci 57:198–207.

Cipolletta S, Beccarello A, Galan A. 2012. A psychological perspective of eye floaters. Qual Health Res 22:1547–1558.

Garcia GA, Khoshnevis M, Yee KMP, Nguyen-Cuu J, Nguyen JH, Sebag J. 2016. Degradation of contrast sensitivity function following posterior vitreous detachment. Am J Ophthalmol 172:7–12.

Goodman J. 1996. Introduction to Fourier Optics, 2nd edition. New York, NY: McGraw-Hill, 38–39.

Ivanova T, Jalil A, Antoniou Y, Bishop PN, Vallejo-Garcia JL, Patton N. 2016. Vitrectomy for primary symptomatic vitreous opacities: An evidence-based review. Eye 30:645–655.

Kapilevich BY, Harmer SW, Bowring NJ. 2014. Non-Imaging Microwave and Millimetre-Wave Sensors for Concealed Object Detection. Boca Raton, FL: CRC Press. pp. 156–160.

Kaymak H. 2017. Are there alternatives for treating floaters? Available from https://www.healio.com/news/ophthalmology/20171016/are-there-alternatives-for-treating-floaters [Last accessed 28 September 2021].

Kim JK, Lin JC. 1998. Successive order scattering transport approximation for laser propagation in whole blood medium. IEEE Trans Biomedical Engineering 45:505–510.

Lesmes LA, Lu ZL, Baek J, Albright TD. 2010. Bayesian adaptive estimation of the contrast sensitivity function: The quick CSF method. J Vis 10:1–21.

Lin JC, Guy AW. 1974. A note on the optical scattering characteristics of whole blood. IEEE Trans Biomedical Engineering 21:43–45.

Luff AJ, O'Donnell C. 2018. Contemporary management options for symptomatic vitreous floaters. Available from https://www.opticianonline.net/cet-archive/5143 [Last accessed 28 September 2021].

Mamou J, Wa CA, Yee KM, Silverman RH, Ketterling JA, Sadun AA, Sebag J. 2015. Ultrasound-based quantification of vitreous floaters correlates with contrast sensitivity and quality of life. Invest Ophthalmol Vis Sci 56:1611–1617.

Maqsood F. 2017. Effects of varying light conditions and refractive error on pupil size. Cogent Med 4:1338824.

Mezouari A, Harvey AR. 2003. Validity of Fresnel and Fraunhofer approximations in scalar diffraction. J Opt A Pure Appl Opt 5:86–91.

Milston R, Madigan MC, Sebag J. 2016. Vitreous floaters: Etiology, diagnostics, and management. Surv Ophthalmol 61:211–227.

Palanker D. 2013. Optical properties of the eye. Available from https://www.aao.org/current-insight/optical-properties-of-eye [Last accessed 28 September 2021].

Pappas TN, Safranek RJ, Chen J, Bovik A. 2005. Handbook of Image and Video Processing, second edition. New York, NY: Academic Press. 939–959.

Pelli DG, Bex P. 2013. Measuring contrast sensitivity. Vision Res 90:10–14.

Rytov SM. 1956. Electromagnetic properties of a finely stratified medium. Sov Phys JETP 2:466–475.

Scholkmann F, Kleiser S, Metz AJ, Zimmermann R, Pavia JM, Wolf U, Wolf M. 2014. A review on continuous wave functional near-infrared spectroscopy and imaging instrumentation and methodology. Neuroimage 85:6–27.

Sebag J. 2020. Vitreous and vision degrading myodesopsia. Prog Ret Eye Res 79:100847.

Sebag J. 2011. Floaters and the quality of life. Am J Ophthalmol 152:3–4.

Sebag J. 1989. The Vitreous: Structure, Function, and Pathobiology. New York, NY: Springer-Verlag. pp. 85–90.

Sebag J, Yee KM, Wa CA, Huang LC, Sadun AA. 2014. Vitrectomy for floaters: Prospective efficacy analyses and retrospective safety profile. Retina 34:1062–1068.

Sekar SKV, Bargigia I, Mora AD, Taroni P, Ruggeri A, Tosi A, Pifferi A, Farina A. 2017. Diffuse optical characterization of collagen absorption from 500 to 1700 nm. J Biomed Opt 22:015006.

Serpetopoulos CN, Korakitis RA. 1998. An optical explanation of the entoptic phenomenon of 'clouds' in posterior vitreous detachment. Ophthalmic and Physiol Opt 18: 446–451.

Sommerville DN. 2015. Vitrectomy for vitreous floaters: Analysis of the benefits and risks. Curr Opin Ophthalmol 26:173–176.

Wagle AM, Lim WY, Yap TP, Neelam K, Au, Eong KG. 2011. Utility values associated with vitreous floaters. Am J Ophthalmol 152:60–65.

Watson AB, Ahumada AJ, Jr. 2005. A standard model for foveal detection of spatial contrast. J Vis 5:717–740.

Watson AB, Yellott JI. 2012. A unified formula for light-adapted pupil size. J Vision 12:112.

Wells-Gray EM, Choi SS, Bries A, Doble N. 2016. Variation in rod and cone density from the fovea to the mid-periphery in

healthy human retinas using adaptive optics scanning laser ophthalmoscopy. Eye 30:1135–1143.

Wu RH, Jiang JH, Gu YF, Moonasar N, Lin Z. 2020. Pars plana vitrectomy relieves the depression in patients with symptomatic vitreous floaters. Int J Ophthalmol 13:412–416.

Yariv A. 1997. Photonics: Optical Electronics in Modern Communications. New York, NY: Oxford University Press. pp. 30–33.

Zeydanli EO, Parolini B, Ozdek S, Bopp S, Adelman RA, Kuhn F, Gini G, Sallam AB, Aksakal N. 2020. EVRS floaters study group, management of vitreous floaters: An international survey the European vitreoretinal society floaters study report. Eye 34:825–834.

Zou H, Liu H, Xu X, Zhang X. 2013. The impact of persistent visually disabling vitreous floaters on health status utility values. Qual Life Res 22:1507–1514.